Nanostructured Functional Materials

In Situ Incorporation of 2-(2-Hydroxyphenyl)benzothiazole within FAU Colloidal Crystals**

Svetlana Mintova, Vincent De Waele, Uli Schmidhammer, Eberhard Riedle,* and Thomas Bein**

Novel nanostructured functional materials can be constructed by encapsulation of optically active guests in microporous hosts. Incorporation of organic molecules inside the cages of zeolites permits the control of both their molecular and optical properties. To achieve this goal, it is essential to accommodate specific molecules within the voids of the zeolite structures and to create nanosized assemblies such as thin films, layers, or monolith structures for specific applications. Generally, the microporous materials used for the preparation of nanostructured assemblies are synthesized in colloidal form from clear aluminosilicate or aluminophosphate solutions, which results in a mean particle size in the range of about 20–600 nm.[1–5] Nanoscale organosilicate clusters in the precursor solutions used for the synthesis of colloidal zeolites have been observed with different techniques.[6–10] Nanoscale amorphous gel particles (with a size of 5–50 nm) are formed in the precursor solutions before long-range crystalline order is established.[3,4] Based on these insights, the encapsulation of additional organic molecules in the crystalline internal voids of zeolite structures should be possible by direct incorporation from the precursor colloidal solutions. Moreover, colloidal molecular sieves with particle sizes in the nanometer range can have high colloidal stability in different solvents with respect to further agglomeration and sedimentation. These features make the encapsulation of functional optical molecules in nanoscale zeolite suspensions an attractive synthetic goal. Such suspensions are 1) promising systems for optical investigations of host–guest interactions, and 2) interesting precursors for the construction of nanostructured assemblies such as optical coatings and selective chemical sensors. The application of nanosized zeolites opens up possibilities for the preparation of homogeneous zeolite films on many different supports, as well as inert substrates, by efficient spin-coating of stable colloidal solutions. The generation of defined porous nanocrystals with encapsulated, optically active guests provides a route to two-dimensional functional constructs for further applications, for example, in the area of optical sensors.

Molecules with excited-state intramolecular proton-transfer (ESIPT) properties constitute a promising family of potential guests in functionalized zeolite materials for applications in the area of UV filtering,[11] sensing,[12] or even molecular switching. Among the different ESIPT systems, the HBX dyes (X = S,O or NH for 2-(2-hydroxyphenyl)benzothiazole (HBT), -benzooxazole, or -benzimidazole systems, respectively) have received particular attention, and their properties are being extensively studied regarding their steady-state[13–18] and time-dependent behavior.[19] The photophysical properties of these compounds are strongly dependent on the polar and protic character of the solvent that influences the relative stability of different tautomers. In addition to their potential as molecular devices, the high sensitivity of HBX dyes to their surroundings renders them interesting probes for the specific microenvironment of the zeolite host.

Herein, we report on the in situ incorporation of HBT inside the supercages of nanosized FAU zeolites as a co-template from a precursor colloidal solution.

Nanosized FAU crystals were prepared from colloidal solutions with (HBT–FAU) and without HBT (FAU) under hydrothermal conditions (see Experimental Section). According to X-ray powder diffraction analysis, both samples correspond to the FAU zeolite-type structure (Figure 1).[4] Dynamic light scattering (DLS) studies reveal that the FAU and HBT–FAU zeolite suspensions contain only monodisperse particles with a mean hydrodynamic radius r of 60 nm and 80 nm, respectively. Figure 2 shows the distribution function analysis (DFA) data of these two colloidal suspensions. The crystalline nature and the morphology of these particles were confirmed with transmission electron microscopy (TEM). The TEM image in the inset in Figure 2 shows well-defined octahedral crystals (ca. 60 nm in size) and crystalline fringes corresponding to the FAU structure. The HBT–FAU crystals show a slight increase in the particle size from 60 to 80 nm (not shown).

[*] Dr. S. Mintova, Prof. Dr. T. Bein
Department of Chemistry
University of Munich
Butenandtstrasse 5–11, 81377 Munich (Germany)
Fax: (+49) 89-2180-77622
E-mail: svetlana.mintova@cup.uni-muenchen.de
tbein@cup.uni-muenchen.de
Prof. Dr. E. Riedle, Dr. V. De Waele, U. Schmidhammer
Lehrstuhl für BioMolekulare Optik
University of Munich
Oettingenstrasse 67, 80538 Munich (Germany)
Fax: (+49) 89-2180-9202
E-mail: eberhard.riedle@physik.uni-muenchen.de

[**] This research was supported by a Marie Curie Fellowship of the European Community program (contract no. HPMFCT-2000-00684).

 DOI: 10.1002/ange.200219900

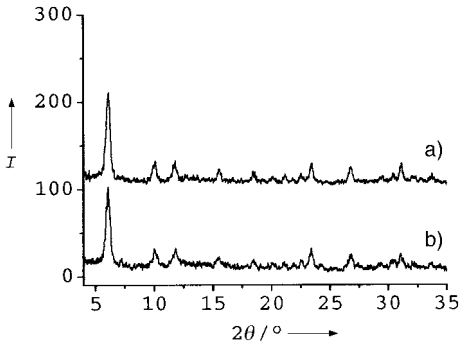

Figure 1. X-ray powder diffraction patterns of a) pure FAU and b) HBT–FAU nanocrystals.

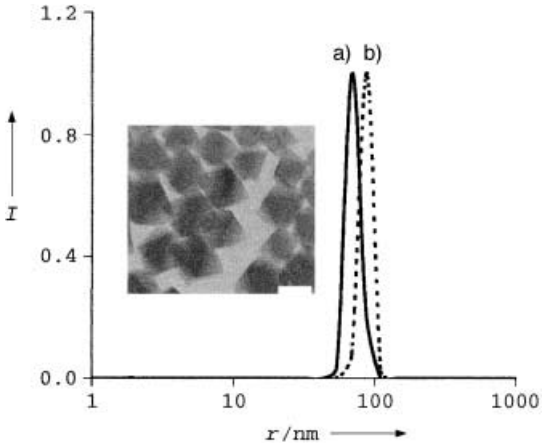

Figure 2. Distribution function analysis data based on DLS of a) pure FAU and b) HBT-FAU nanocrystals. Inset: TEM image of FAU nanocrystals; bar = 20 nm.

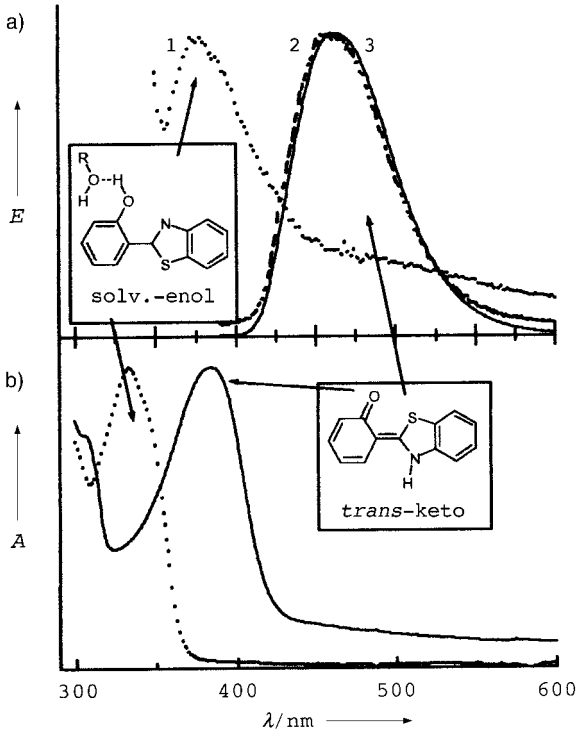

Figure 3. a) Normalized emission spectra of HBT in ethanol excited at 340 nm (trace 1) and at 380 nm (trace 2), and in the HBT–FAU sample (trace 3) excited at 380 nm. b) Absorption spectra of HBT in ethanol (•••••) and in the HBT–FAU sample (——). Insets: the solv-enol and *trans*-keto HBT conformations assigned to the observed absorption and emission spectra.

The absorption and emission spectra of the HBT–FAU and pure HBT in ethanol are depicted in Figure 3. The spectroscopic properties of HBT incorporated in FAU crystals change significantly with respect to those of HBT dissolved in pure ethanol. In ethanol HBT absorbs at 335 nm (Figure 3b), while its emission spectrum (excited at 340 nm; Figure 3a, trace 1) exhibits a maximum at 370 nm. In the HBT–FAU sample, the absorption band is at 380 nm (Figure 3b), while the emission (excited at 380 nm; Figure 3a, trace 3) exhibits a strong band centered at 465 nm. In ethanol, the strong absorption band of HBT was assigned to the solvated enol (solv-enol) tautomer, and the keto tautomer is present in trace quantities.[13–15] The keto tautomer absorbs at 380 nm and its emission is centered at 460 nm (Figure 3a, trace 2). From the comparison of the spectra shown in Figure 3a, it is evident that the solv-enol tautomer is not present in the HBT–FAU sample. Instead, in HBT-FAU we observe an absorption band at 380 nm that is characteristic of the keto tautomer. Moreover, since the emission excited at 380 nm is virtually identical for both the HBT–FAU sample and the keto trace species in ethanol (see Figure 3a, trace 2 and 3), we attribute the spectroscopic properties of HBT–FAU to the presence of the keto tautomer. Owing to the excellent match of the above spectral signatures, the alternative interpretation based on the formation of the HBT anion is excluded. Notably, the UV/Vis spectra clearly indicate that after preparation of HBT–FAU, the HBT molecules are only located in the zeolite, and not in the ethanolic solution.

As mentioned above, the properties of HBT are very sensitive to the surroundings of the molecule. This sensitivity derives from the competition between intra- and intermolecular hydrogen bonding, as well as from polarity effects that influence the relative stability of the different conformations and tautomers. The UV/Vis data clearly shows that no ESIPT process, which would require the enol ground state, occurs in the voids of zeolite Y. As mentioned above, the HBT–FAU absorbs at longer wavelength than the enol (380 nm for HBT–FAU versus 335 nm for HBT in ethanol). In addition, the usual strong red shift of the emission, which is the typical signature of the ESIPT process, was not observed. For example, in cyclohexane, the maximum of the ESIPT emission is observed at 540 nm.[19a] Thus the intramolecular hyrogen bond of HBT is broken in the zeolite, and HBT in the inner space of the FAU zeolite interacts with its microenvironment (zeolite framework or other guest molecules).

To characterize the surroundings of HBT and to provide experimental evidence for the incorporation of HBT within the FAU nanosized crystals, Raman spectra of pure FAU and HBT–FAU samples were recorded (Figure 4). Both spectra are dominated by the Raman lines assigned to the presence of tetramethylammonium (TMA) ions.[20] Moreover, numerous

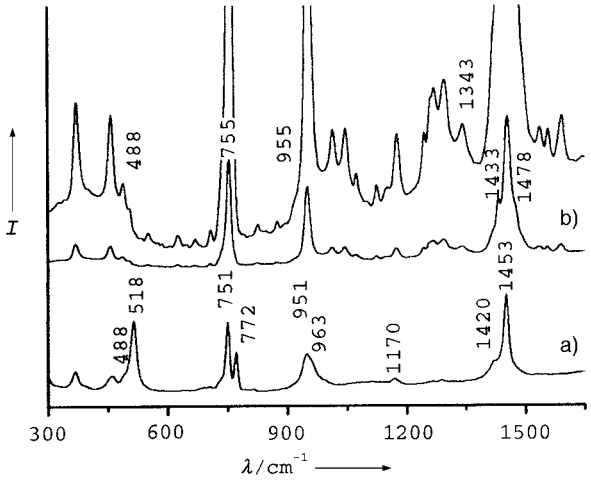

Figure 4. Raman spectra of a) FAU and b) HBT–FAU samples.

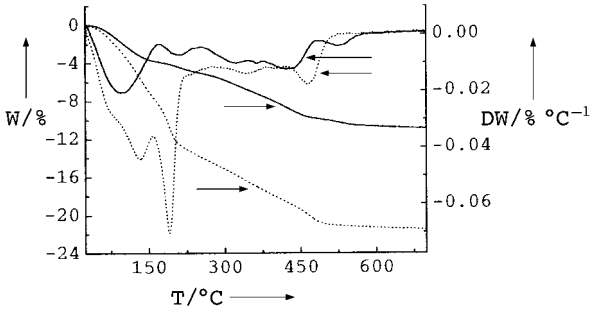

Figure 5. Thermogravimetric (W = weight loss)/differential thermogravimetric data (DW = differential weight loss) of pure FAU (——) and HBT–FAU nanocrystals (•••••) (heating rate 10 K min^{-1}, in air).

new lines due to the presence of HBT in the zeolite are observed in the Raman spectrum of the HBT–FAU sample. For example, the three Raman lines of HBT incorporated within the FAU nanocrystals at 1343, 1433, and 1478 cm^{-1} are associated with the enol–HBT lines in ethanol at 1320, 1440, and 1464 cm^{-1},[21] respectively. These three bands involve C–C stretching modes and notably the biaryl central C–C bond.[21] The displacement of the above Raman lines is attributed to the electronic reorganization of the molecule, as expected to occur during the tautomerization.

The Raman data confirm the presence of HBT in the HBT–FAU sample and also reveal a modification of the TMA ion surroundings when the faujasite is synthesized in presence of HBT. The Raman spectrum of the FAU sample displays several strong lines between 500 and 1000 cm^{-1}, whereas only two strong lines are present in the same region in the corresponding spectrum of the HBT–FAU sample. The presence of double lines around 750 and 950 cm^{-1} reflects the existence of two different conformations of the TMA ion in the FAU structure, while only two single lines at 755 and 955 cm^{-1} are observed in the Raman spectrum of HBT–FAU. This observation suggests that only one conformation or local environment of the TMA ion is present in HBT–FAU.

To probe the association of HBT and TMA molecules with the pure FAU and HBT–FAU samples, we performed thermogravimetric analysis (TGA) of washed and freeze-dried samples (Figure 5). The weight loss of the FAU sample in the temperature range 200–600 °C is 6 wt %, which is attributed to combustion of TMA (weight loss below 200 °C is attributed to the removal of zeolite-type water molecules). The TMA template in pure FAU decomposes in at least two steps, that is, at 420 and 510 °C, which may suggest different local environments of the TMA template in the FAU structure. In contrast to the thermal degradation of the pure FAU sample, that of the TMA and HBT occurs predominantly at 450 °C (9 wt %). These results point to the different local environments of the organic molecules in the two samples.

In conclusion, the dye 2-(2-hydroxyphenyl)benzothiazole (HBT) was successfully incorporated into the voids of nanoscale FAU zeolites. The mechanism of inclusion appears to involve a complex interaction between the TMA ion and HBT that occurs during the templating phase of the synthesis. UV/Vis and Raman spectroscopic data reveal that the *trans*-keto tautomer of HBT is stabilized inside this large-pore molecular sieve. The *trans*-keto tautomer exhibits highly intensive fluorescence in the zeolite, as compared to the *cis*-keto tautomer formed in solution during the ESIPT process. This indicates a profound modification of the excited-state properties, and especially the internal conversion mechanism associated with the ESIPT process. Further studies are in progress to elucidate the time-resolved photophysics of these and related functional host–guest systems.

Experimental Section

Nanosized HBT–FAU and pure FAU crystals were prepared from clear precursor solutions with the following molar compositions: FAU: 5.5 $(TMA)_2O$:2.3 Al_2O_3:10 SiO_2:570 H_2O; HBT-FAU: 0.05 HBT:2.7 $(TMA)_2O$:2.3 Al_2O_3:10 SiO_2:100 H_2O:400 EtOH.

Precursor solution for FAU: Tetramethylammonium hydroxide pentahydrate ($TMAOH{\cdot}5H_2O$) (5.18 g) was added to an aqueous solution (26.68 g water) of aluminum isopropoxide (2.44 g) to give a clear solution. Then a second solution (5.1 g) containing silica sol (30 wt %, particle size ~5 nm) was added under stirring.

Precursor solution for HBT–FAU: Tetramethylammonium hydroxide pentahydrate ($TMAOH{\cdot}5H_2O$) (2.54 g) was added to an aqueous solution (4.68 g water) of aluminum isopropoxide (2.44 g) to give a clear solution. Commercially available HBT was purified by recrystallization, dissolved in ethanol (0.030 g in 47.9 g EtOH), and then was mixed with the silica sol (5.1 g).

Synthesis of FAU[4] and HBT–FAU: The above precursor solutions were further stirred for about 60 min at room temperature. The final precursor solutions were aged on an orbital shaker (180 rpm) at room temperature for 24 h prior to further crystallization at 90 °C for 28 h. The nanosized FAU crystals resulting from this hydrothermal treatment were purified by separation from the mother liquid by three steps of centrifugation (20000 rpm, 60 min). After each step the nanoparticles were redispersed in ethanol (98 %, Aldrich) by using an ultrasonic bath for 3 h; the concentration of the solid nanocrystals in the final suspensions was about 1.5 wt %. The X-ray diffraction data were collected on a Scintag XDS 2000 diffractometer using $Cu_{K\alpha}$ radiation. The TG measurements were performed with a Setaram TG-ATD LABSYS thermal analyzer. In situ dynamic light scattering was used (ALV-NIBS/HPPS) to investigate the particle size distributions at room temperature and upon hydrothermal treatment at 90 °C. The distribution function analysis data and high-resolution transmission electron microscopy (HR-TEM)

data provided information about the size and crystalline nature of the nanosized particles. Raman spectra of the purified and freeze-dried HBT–FAU and FAU samples were recorded on a Bruker Equinox 55 FT-Raman spectrometer (500 mW at 1064 nm; collection time 180 min). The steady-state absorption of the ethanolic solutions of HBT–FAU and FAU were measured with a Specord S100 spectrometer from Analytik Jena, while the steady-state emission spectra were recorded with a fluorescence spectrometer type Spex-Fluorolog-2.

Received: August 6, 2002
Revised: January 15, 2003 [Z19900]

Keywords: fluorescence · inclusion chemistry · microporous materials · zeolites

[1] a) B. J. Schoeman, *Zeolites* **1997**, *18*, 97; b) B. J. Schoeman, *Microporous Mesoporous Mater.* **1998**, *22*, 9,
[2] C. E. A. Kirschhock, R. Ravishankar, F. Verspeurt, P. J. Grobet, P. A. Jacobs, J. A. Martens, *J. Phys. Chem. B* **1999**, *103*, 4965.
[3] S. Mintova, N. Olson, V. Valtchev, T. Bein, *Science* **1999**, *283*, 958.
[4] S. Mintova, N. Olson, T. Bein, *Angew. Chem.* **1999**, *111*, 3400; *Angew. Chem. Int. Ed.* **1999**, *38*, 3201.
[5] S. Mintova, N. H. Olson, J. Senker, T. Bein, *Angew. Chem.* **2002**, *114*, 2670; *Angew. Chem. Int. Ed.* **2002**, *41*, 2558.
[6] C. E. A. Kirschhock, R. Ravishankar, P. A. Jacobs, J. A. Martens, *J. Phys. Chem. B* **1999**, *103,* 11021.
[7] P. P. E. A. de Moor, T. P. M. Beelen, R. A. van Santen, *J. Phys. Chem. B* **1999**, *103*, 1639.
[8] Q. Li, B. Mihailova, D. Creaser, J. Sterte, *Microporous Mesoporous Mater.* **2001**, *43,* 51.
[9] C. E. A. Kirschhock, V. Buschmann, S. Kremer, R. Ravishankar, C. J. Y. Houssin, B. L. Mojet, R. A. van Santen, P. J. Grobet, P. A. Jacobs, J. A. Martens, *Angew. Chem.* **2001**, *113,* 2707; *Angew. Chem. Int. Ed.* **2001**, *40*, 2637.
[10] O. Regev, Y. Cohen, E. Kehat, Y. Talmon, *Zeolites* **1994**, *14*, 314.
[11] a) P. T. Chou, M. L. Martinez, S. L. Studer, *Appl. Spectrosc.* **1991**, *45*, 918; b) J. Keck, H. E. A. Kramer, H. Port, T. Hirsch, P. Fischer, G. Rytz, *J. Phys. Chem.* **1996**, *100*, 144468; c) M. Stein, J. Keck, F. Waiblinger, H. E. A. Kramer, A. Hartschuh, H. Port, D. Leppard, G. Rytz, *J. Phys. Chem. A* **2002**, *106*, 2055.
[12] Y. Kubo, S. Maeda, S. Tokita, M. Kubo, *Nature* **1996**, *382*, 522.
[13] G. J. Woolfe, M. Melzig, S. Schneider, F. Dörr, *Chem. Phys.* **1983**, *77*, 213.
[14] M. Mosquera, J. C. Penedo, M. C. Rios Rodriguez, F. R. Rodriguez-Prieto, *J. Phys. Chem.* **1996**, *100*, 5398.
[15] E. L. Robert, J. Dey, I. M. Warner, *J. Phys. Chem. A* **1997**, *101*, 5296.
[16] T. Elsaesser, B. Schmetzer, *Chem. Phys. Lett.* **1987**, *140*, 293.
[17] C. S. Potter, R. G. Brown, *Chem. Phys. Lett.* **1988**, *153*, 7.
[18] M. M. Henary, C. J. Fahrni, *J. Phys. Chem. A* **2002**, *106*, 5210.
[19] a) W. Frey, F. Laermer, T. Elsaesser, *J. Phys. Chem.* **1991**, *95*, 10391; b) C. Chudoba, E. Riedle, M. Pfeiffer, T. Elsaesser, *Chem. Phys. Lett.* **1996**, *263*, 622; c) S. Lochbrunner, A. J. Wurzer, E. Riedle, *J. Chem. Phys.* **2000**, *112*, 10699; d) S. Lochbrunner, K. Stock, V. De Waele, E. Riedle, *Femtochemistry and Femtobiology: Ultrafast Dynamics in Molecular Science* (Eds.: A. Douhal, J. Santamaria), World Scientific Publishing House, Singapore, **2002**, p. 202.
[20] a) P. K. Dutta, B. Del Barco, D. C. Shieh, *Chem. Phys. Lett.* **1986**, *127*, 200; b) B. D. McNicol, G. T. Pott, K. R. Loos, *J. Phys. Chem.* **1972**, *76*, 3388; c) S. B. Hong, *Microporous Mater.* **1995**, *4*, 309.
[21] M. Pfeiffer, K. Lenz, A. Lau, T. Elsaesser, *J. Raman Spectrosc.* **1995**, *26*, 607.
[22] J. Gao, L. W. Chou, A. Auerbach, *Biophys. J.* **1993**, *65*, 43.

